Prediction and optimization of ion transport characteristics in nanoparticle-based electrolytes using convolutional neural networks

Sanket Kadulkar,[†] Michael P. Howard,[†] Thomas M. Truskett,[*,‡] and Venkat Ganesan[*,†]

[†]McKetta Department of Chemical Engineering, University of Texas at Austin, Austin, Texas 78712, USA

[‡]McKetta Department of Chemical Engineering and Department of Physics, University of Texas at Austin, Austin, Texas 78712, USA

E-mail: truskett@che.utexas.edu; venkat@che.utexas.edu

Abstract

We develop a convolutional neural network (CNN) model to predict the diffusivity of cations in nanoparticle-based electrolytes, and use it to identify the characteristics of morphologies which exhibit optimal transport properties. The ground truth data is obtained from kinetic Monte Carlo (kMC) simulations of cation transport parameterized using a multiscale modeling strategy. We implement deep learning approaches to quantitatively link the diffusivity of cations to the spatial arrangement of the nanoparticles. We then integrate the trained CNN model with a topology optimization algorithm for accelerated discovery of nanoparticle morphologies that exhibit optimal cation diffusivities at a specified nanoparticle loading, and we investigate the ability of the CNN model to quantitatively account for the influence of interparticle spatial correlations on cation diffusivity. Finally, using data-driven approaches, we explore how simple descriptors of nanoparticle morphology correlate with cation diffusivity, thus providing a physical rationale for the observed optimal microstructures. The results of this study highlight the capability of CNNs to serve as surrogate models for structure–property relationships in composites with monodisperse spherical particles, which can in turn be used with inverse methods to discover morphologies that produce optimal target properties.

1 INTRODUCTION

Nanocomposites comprising spherical nanoparticles dispersed in polymeric matrices or liquid hosts have emerged as a promising class of materials for a broad range of applications. The introduction of nanoparticles can enhance the ionic conductivity,[1,2] mechanical strength,[3–5] optoelectronic properties,[6,7] and separation performance[8–10] of the host material. Since the mechanisms underlying the observed property improvements remain poorly understood,[11,12] there is interest to find new approaches to predict the nanoparticle loading and microstructure characteristics that optimizes the properties of interest.

Although nanoparticle loading is known to be an important factor influencing nancomposite properties, experimental and theoretical studies have found that the spatial organization of the nanoparticles also strongly influences macroscopic behavior. For instance, Jana and coworkers reported polybenzimidazole nanocomposite systems with morphology-dependent proton conduction[13–15] and storage modulus[14] properties at a fixed nanoparticle loading. In their studies, the characteristic structure of the dispersed nanoparticles was altered by modifying the nanoparticle surface with various functional groups. Similarly, Akcora et al.[16] reported tunability in mechanical properties of polymer nanocomposites at a fixed nanoparticle volume fraction by varying the grafting density and molecular weight of tethered chains, and attributed such behavior to the resulting modulation of the nanoparticles' self-assembled structure. A recent mesoscale simulation study of ours[17] highlighted the potential for modifying nanoparticles structure to significantly influence the tracer diffusivity through nanocomposite gels in the presence of interface-assisted transport pathways.

A key challenge in any of these efforts is to determine specific nanoparticle microstructures that are optimal for targeted macroscopic properties. Knowledge of such microstructures could provide new mechanistic insights, and in addition facilitate discovery of nanoparticle interactions that are most promising for experimental realization of the microstructures using inverse methods.[18,19] Due to the high-dimensional nature of the relevant search spaces, which in principle includes all possible configurations of the nanoparticles, experimental screening of candidate microstructures is often practically intractable. An attractive alternative is to solve for the microstructures using a topology optimization algorithm[20–23] that leverages structure–property predictions from a computationally tractable surrogate model.

In this context, data-driven models have recently emerged as a promising approach for quantifying the structure–property relationships in two-phase composites. Specifically, machine learning approaches have been employed to develop surrogate models for quantitative prediction of macroscopic properties with binary composite microstructure as input, represented by either low-dimensional structural descriptors or as representative volume ele-

ments. In the studies pertaining to the former, the hand-crafted features representing the microstructure are linked to an associated property using a regression-based model[24–30] or artificial neural network.[31,32] For the latter case, convolutional neural networks (CNNs)[33] are employed to extract important features from the digitized images of composite microstructures, generated by stochastic growth of grains[34–38] or by random assignment of numbers in the uniformly voxelized grids,[39–41] in order to predict the effective property of interest.

Motivated by the above advances, we hypothesize that machine learning techniques can be similarly applied to correlate the properties of nanocomposites reinforced with spherical nanoparticles to their microstructure. Further, integrating such structure–property linkages with microstructure optimization algorithms could significantly accelerate the exploration of the relevant high-dimensional configuration spaces to identify nanoparticle morphologies possessing optimal characteristics.

In this study, we demonstrate the above strategy by the application of deep learning approaches for predicting the diffusion coefficient of cations in single-ion conducting nanoparticle-based electrolytes. The choice of the system was inspired by a recent study of ours[42] probing the mechanistic bases for ion transport observations reported in these electrolytes. Our results in such a context were consistent with the reported experimental behavior of electrolytes comprising silica nanoparticles, cofunctionalized with polyethylene glycol ligands and tethered anionic species coupled to Li^+ ions, dispersed in ion-conducting tetraglyme solvent.[43,44] Our simulation results suggested that ionic conductivity in such systems is primarily controlled by cation diffusion along functionalized nanoparticle surfaces. With such mechanistic findings, the connectivity of the cation diffusion pathways is hypothesized to be dependent on the spatial arrangement of the nanoparticles, and it would be desirable to identify the morphologlies that exhibit optimal cation diffusivities.

In this work, we develop a three-dimensional (3D) CNN model to capture the nonlinear mapping between the nanoparticle microstructure and the resulting cation diffusivity. The structure–property linkages established using the CNN model exhibit better accuracy

4

for predicting diffusivities compared to that using other deep learning models based on physics-inspired approaches. We then use the trained CNN model to perform topology optimization for identifying nanoparticle configurations that can potentially exhibit a wider range of diffusivities. We explore the extent to which the deep learning model captures the relevant physical information influencing cation diffusivity based on the CNN predictions for microstructures with different nanoparticle volume fractions. Lastly, by analyzing the influence of physics-inspired structural descriptors on cation diffusivity, we discuss the structural characteristics of the optimal microstructures and provide a physical rationale for the optimal cation diffusivities exhibited by these structures. While the present study is inspired by the nanoparticle-based electrolyte system, the methods and ideas presented in this work can be easily adapted to establish quantitative structure–property relationships and identify optimal morphologies in other nanoparticle-based systems.

The rest of the article is organized as follows. Details of the dataset generation, training of the CNN model, and topology optimization algorithm are provided in Section 2. The results pertaining to the predictive performance of the model, and its ability to discover optimal microstructures when integrated with a topology optimization algorithm, are presented in Section 3. By modifying the inputs to the CNN model, we provide a physical interpretation of its learning aspects in Section 4. We report on the correlation of physics-inspired structural descriptors with cation diffusivity using the data-driven approaches in Section 5. Section 6 concludes the paper with a summary of our findings and provides an outlook regarding the generality of our methodology to train CNN models for exploring structure–property relationship in two-phase composites doped with spherical nanoparticles.

2   DATASETS AND METHODS

Figure 1 illustrates the workflow implemented in this study. In this section, we discuss the methodologies adopted to generate the training dataset, train the CNN-based deep learning
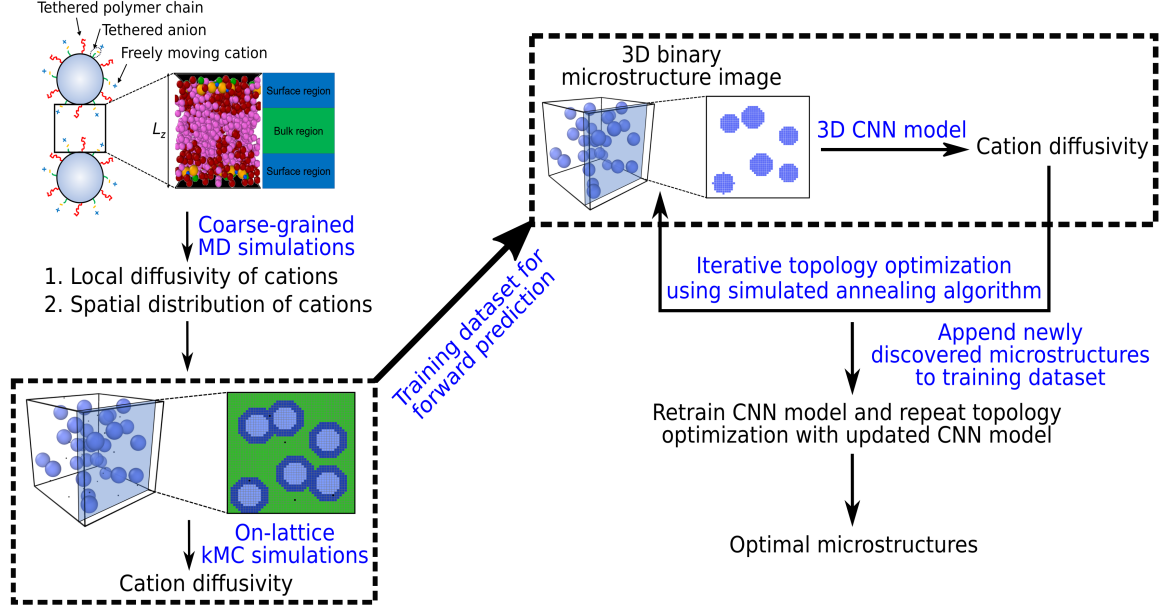
Figure 1: Flowchart for CNN-assisted prediction and optimization of cation diffusivity in nanoparticle-based electrolytes.

model, and integrate the CNN model with the topology optimization algorithm for prediction and optimization of cation diffusivity in nanoparticle-based electrolytes.

The ground truth data used in the training process is generated via a multiscale simulation framework which computes the cation diffusivities for a large dataset of diverse microstructures at a fixed nanoparticle loading. Section 2.1 describes the physics-inspired strategy employed to generate the dataset of diverse microstructures at a fixed nanoparticle loading to span a wide range of cation diffusivities for training the machine learning models. Section 2.2 discusses the methodology to compute ground truth cation diffusivity for a given nanoparticle microstructure. The details pertaining to the CNN architecture and the topology optimization runs are presented in Section 2.3 and Section 2.4, respectively. An improved predictive model is developed by appending the structures identified using the optimization strategy (as well as the corresponding simulated cation diffusivities) to the initial training dataset, and subsequently retraining the CNN model as discussed in Section 2.5.

6

2.1 Generation of Microstructure Dataset

Training a CNN model to predict the diffusivity of cations in nanoparticle-based electrolytes requires generating a large dataset of diverse nanoparticle topologies exhibiting a wide range of cation diffusivities. The dataset itself includes thousands of configurations of nanoparticles, represented in the form of 3D digitized images, and the values of the associated cation diffusivities, calculated using the mesoscale kMC simulations discussed in Section 2.2.

The number of nanoparticles considered for the microstructures in the dataset should be large enough to capture the wide variety of possible topologies spanning length scales relevant for cation transport. At the same time, the microstructures should be small enough such that the ground truth diffusivities for a large number of distinct particle configurations can be calculated at a reasonable computational cost. In our study, we balance these considerations by using configurations of $N = 91$ identical nonoverlapping nanoparticles of diameter σ_{NP} in a cubic box of size L with periodic boundary conditions. The nanoparticle volume fraction $N\pi\sigma_{\mathrm{NP}}^3/(6L^3)$ is fixed to be 0.1 for all the structures. Such a choice of volume fraction allows for realizing a variety of nanoparticle configurations exhibiting broad range of cation diffusivities.

To achieve high prediction accuracy for a wide variety of morphologies in the configurational space screened during the topology optimization runs, a large training dataset containing diverse microstructures and large variation of cation diffusivities is required. However, only a relatively narrow distribution of cation diffusivities was obtained for the configurations generated using random sequential adsorption (RSA) algorithm[45] (supporting results in SI, Section S2) which ensures nonoverlap between nanoparticles in the microstructure. Accordingly, we modify the standard RSA algorithm with the addition of physics-based modifications described below to ensure that configurations corresponding to a wide range of cation diffusivities are included.

For the ion transport model considered here, we previously reported[42] that the *average nearest particle distance* and *percolation* of the nanoparticles are significant aspects influenc-

ing diffusivity. Briefly, the former dictates the "connectivity" between adjacent nanoparticles and correspondingly the mobility of cations while hopping from the surface of a nanoparticle to that of its neighbor. In the model, there exists an ideal range for the distance between adjacent particles to facilitate cation transport; separations too large disrupt "contact" between neighboring nanoparticle surface regions and separations too close result in interdigitation of nanoparticle surface functional groups that reduces cation mobility. Percolation, which characterizes the spatial extent of particle connectivity and thereby the corresponding surface transport pathways, correlates positively with cation diffusivity.

Given these physical considerations, we modify the standard RSA algorithm to generate different microstructures that represent a wide range of average nearest particle distances and extents of percolation. Specifically, we generate 5304 structures by randomly inserting each new particle within a specified range of distances from the previous particle (In SI, Section S2 we present more details on what different constraint distances were used). 2166 additional configurations were generated using RSA algorithm with a further constraint that explicitly disrupted percolation in one or more dimensions of the simulation box (more details in SI, Section S2). The dataset also includes 722 structures generated using an RSA algorithm with no constraints. The configuration data is then split randomly into training, validation and test datasets with 4916, 1638, and 1638 microstructures, respectively.

2.2 Model and Simulation Methodology to generate ground truth Labels for Microstructures

Since simulation of nanoparticle-based electrolytes using atomistically detailed molecular models is computationally prohibitive, we use the multiscale simulation framework from our recent study[42] to compute the cation diffusivities for microstructures in the training dataset.

In brief, this multiscale simulation strategy involves using coarse-grained molecular dynamics (MD) simulations to probe the region between two adjacent functionalized nanoparticles. Such simulations provide means for characterizing the effective pair interactions be-

tween functionalized nanoparticles, as well as the spatial distribution of the cations and their local (i.e., position-dependent) diffusivity. This information serves as input for an on-lattice, mesoscale model of the nanoparticle-based electrolyte in which kinetic Monte Carlo (kMC) simulations are used to simulate transport of cations through the given nanoparticle configuration. The bulk diffusivity of cations D_{kMC} is then calculated from the resulting cation trajectories using the Einstein–Smoluchowski relation,

$$D_{\text{kMC}} = \lim_{t \to \infty} \frac{1}{6t} \langle [\mathbf{r}_i(t) - \mathbf{r}_i(0)]^2 \rangle, \tag{1}$$

where $\langle [\mathbf{r}_i(t) - \mathbf{r}_i(0)]^2 \rangle$ is the mean squared displacement of cations at time t.

Due to the large separation of time scales between diffusion of cations and nanoparticles, the nanoparticles are treated as immobile obstacles in the simulations. Further details about the coarse-grained MD and mesoscale kMC simulations are provided in the SI, Section S1.

In the present work, cation diffusion coefficients computed for the microstructures in the training dataset using kMC simulations parameterized with a fixed set of cation local diffusivities and cation-nanoparticle affinities, determined from the coarse-grained MD simulations of our previous study,[42] serve as the ground truth labels. To emphasize the efficacy of employing the combination of CNN model and topology optimization algorithm to identify non-intuitive microstructures with high diffusivities, we define a dimensionless number, $D_{\text{kMC}}^* = D_{\text{kMC}}/D_o$, where D_o is the maximum value of ground truth cation diffusivity in the originally generated dataset.

2.3 Convolutional Neural Network Model

The convolutional neural network (CNN) is a widely-used deep learning approach for computer vision tasks,[46] which utilizes image-like data as input. A typical CNN architecture includes the following different layers: convolutional layers, pooling layers, activation functions and fully connected layers. Convolutional layers extract the spatial features of the
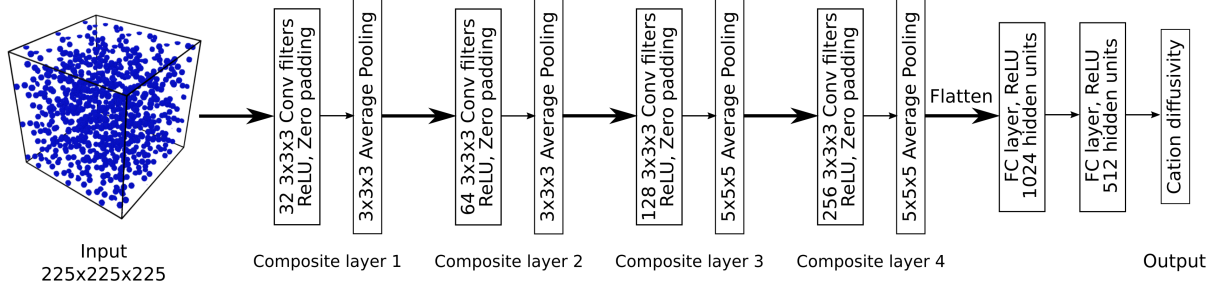
Figure 2: Architecture of the 3D CNN.

input image by applying filters learned from the training dataset. An activation function is usually applied after the convolutional layer to introduce nonlinearity into the network and capture the complex relationship between the inputs and outputs. Pooling layers are added after the activation functions to reduce the dimensions of the feature map outputs from the convolutional layer. Finally, the objective of the fully connected layers is to predict the output value based on the nonlinear combinations of the feature maps from a series of convolution and pooling layers.

The resolution of the CNN input in every direction was chosen to be 5 times lower than the grid size adopted for the on-lattice kMC simulations. Such a resolution sufficiently mitigates discretization effects while maintaining a small enough input size to the CNN models for computational efficiency. Accordingly, all microstructures are first converted to a $75 \times 75 \times 75$ binary images, where voxels corresponding to the region occupied by the nanoparticles are denoted as 1, and 0 is used to index the empty voxels (more details in SI, Section S3). Although the on-lattice kMC simulation models cation transport through the nanoparticle microstructure using periodic boundary conditions, the convolutional layers in the CNN are incapable of capturing the periodic boundary conditions on the spatial volume unless the input image explicitly reflects the periodicity. Since the relevant length scales influencing the transport of cations are typically larger than the dimensions of the nanoparticle microstructure considered in this study, every binary image constructed from the nanoparticle configuration in the cubic box is repeated 3 times in all three directions, and the resulting binary image of size $225 \times 225 \times 225$ is provided as input to the CNN

10

model to better capture the effect of periodic boundary conditions. (Results for the inferior CNN model performance without the repetition of binary image are presented in SI, Section S5.1).

The diameter of a single nanoparticle is approximately the length of 10 voxels in the input image, and convolutional filters of size comparable to multiple nanoparticles are needed to capture interparticle spatial correlations. Convolutional layers with such large filter size also require a relatively large number of filters to effectively account for spatial features incorporating multiple nanoparticles. However, the training process of such CNN models with large datasets is computationally intractable. Instead, we employ a deeper network comprising multiple layers while choosing the convolutional filter size for every layer to be smaller than that of a single nanoparticle, as illustrated in Figure 2. We fix the convolutional filter size to be $3 \times 3 \times 3$ for all the layers. The CNN architecture considered for this study consists of four composite layers, each consisting of a convolution layer, a rectified linear unit (ReLU) activation function, and average pooling layer, followed by two fully connected layers. The number of convolutional filters and neurons in the fully connected layers were decided based on the accuracy of testing set predictions for the respective CNN architectures (results for different CNN architectures presented in SI, Section S5.2).

The CNN models were trained on 4 NVIDIA Tesla V100 GPUs with 16GB RAM for each GPU, using the Keras library[47] built on top of Tensorflow implemented in Python 3.7. The hyperparameters used to train the CNN models are reported in SI, Section S4.

2.4 Topology Optimization using Simulated Annealing

Simulated annealing (SA) is an effective, heuristic algorithm that stochastically searches for the global optimum of an objective function on a landscape where many local optima may be present. The approach has analogies to physical annealing, where a material avoids getting trapped in local energy minima (e.g., defective crystals or glasses) and eventually realizes its lowest energy state (i.e., crystal) by slowly cooling it from high to low temperature.

Earlier studies have utilized SA for solving structural optimization problems with discrete variables.[48–50] In this article, we integrate the trained CNN model with an SA algorithm to navigate the morphological space and identify microstructures exhibiting a wide range of diffusivities. From a design perspective, one may be interested in identifying structures with high diffusivities. However, discovery of low-diffusivity microstructures is also essential for progressively improving the CNN model through their incorporation in the training process as discussed in Section 2.5. Toward these objectives, two independent SA algorithms were employed to find microstructures that maximize (and minimize) the cation diffusivities, naturally leading to the discovery of microstructures with higher (and lower) simulated diffusivities than those for structures in the originally generated dataset.

At each step of the SA algorithm, the center of a nanoparticle is randomly moved to a neighboring voxel in the binary image while ensuring nonoverlap of nanoparticles. When the SA algorithm is used to maximize diffusivity, the probability of accepting the move/transition from structure i to structure j (p_{ij}) is given by:

$$
p_{ij} = \begin{cases} 1, & D^*_{\mathrm{CNN}}(j) \geq D^*_{\mathrm{CNN}}(i) \\ \exp\left[\frac{D^*_{\mathrm{CNN}}(j) - D^*_{\mathrm{CNN}}(i)}{D^*_k}\right], & D^*_{\mathrm{CNN}}(j) < D^*_{\mathrm{CNN}}(i), \end{cases} \tag{2}
$$

where $D^*_{\mathrm{CNN}}(j)$ is the diffusivity for structure j, estimated using the CNN model and normalized by D_o, and D^*_k is a dimensionless control parameter chosen for the kth cycle of the SA algorithm. A geometric cooling profile was adapted for $D^*_k, k = 2, 3, ..., k_{\max}$, described by the formula:

$$
D^*_k = \alpha D^*_{k-1} \tag{3}
$$

where $\alpha = 0.9$ and $D^*_1 = 9.8 \times 10^{-3}$. A similar condition as in Eq. 2 is applied to advance the SA algorithm for minimizing diffusivity, except the diffusivities are replaced by their negative values. The total number of cycles ($k_{\max}$) in the SA algorithms used to maximize and minimize diffusivity were 50 and 100, respectively. 2500 steps of the SA algorithm were

performed for each cycle. To ensure that microstructures from different domains of the structural landscape were screened, we performed 10 independent runs for both SA algorithms with a different initial morphology for each run, generated using the RSA algorithm.

2.5 Retraining the CNN Model

Due to the limited microstructural domains featured in the dataset generated using the methodology discussed in Section 2.1, augmenting the microstructures with those identified from optimizing the CNN model with the SA algorithm, and subsequently retraining the CNN model with the expanded dataset, is expected to improve diffusivity predictions for a wider range of nanoparticle morphologies.[51,52] To this end, cation diffusivities for the structures identified from the topology optimization runs were calculated using our kMC simulation methodology. Specifically, from the structures evaluated during the SA algorithm for maximizing diffusivity, 5000 configurations with uniform distribution of CNN-predicted diffusivities higher than the maximum diffusivity value in the original dataset were chosen randomly, analyzed using the kMC simulations and added to the dataset. Similarly, 2280 structures from the ones explored using the SA algorithm for minimizing diffusivity were evaluated using kMC simulation and appended to the dataset as well. The numbers of training, validation and test data points for the new dataset were 9712, 3240, and 3240, respectively. Following the retraining of the CNN model, the topology optimization process described in Section 2.4 was repeated using the updated CNN model.

3 RESULTS AND DISCUSSION

3.1 CNN Model Performance

In this section, we present results demonstrating the ability of the CNN model to accurately predict cation diffusivity values. The performance of the CNN model is compared with other deep learning models based on physics-inspired approaches. The accuracy of a model
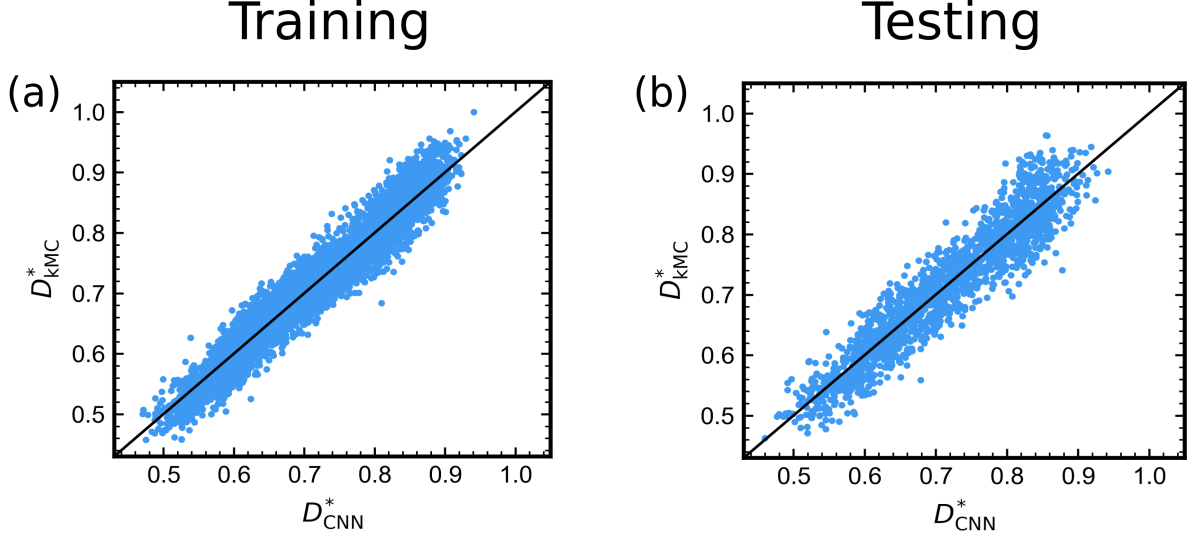
Figure 3: CNN predictions for original dataset. Parity plots of CNN model for (a) training and (b) testing sets.

is reported using the mean squared error (MSE) and mean absolute percentage error (MAPE) which are defined as:

$$MSE = \frac{1}{N} \sum_{i=1}^{N} (y_i - \hat{y}_i)^2 \tag{4}$$

$$MAPE = \frac{1}{N} \sum_{i=1}^{N} \left| \frac{y_i - \hat{y}_i}{\hat{y}_i} \right| \times 100\% \tag{5}$$

where y_i is the value predicted by the model, and $\hat{y}_i$ is the ground truth value.

Figure 3 shows a parity plot between the diffusivities predicted using the best-performing CNN and those calculated using the kMC simulations. We observe that the CNN model predicts the cation diffusivity for the unseen microstructures in the testing set with high accuracy. Moreover, the trained CNN model predicts the cation diffusivity with computational cost of roughly three orders magnitude lower than the kMC simulations.

Next, we compare the performance of the CNN model with other physics-inspired deep learning models (Figure 4) created to establish quantitative structure–property linkages. In the absence of a preexisting analytical model for predicting transport properties in nanoparticle-based composites (for which nanoparticle-surface transport pathways have a strong influence), artificial neural network models were trained with simple, structural de-
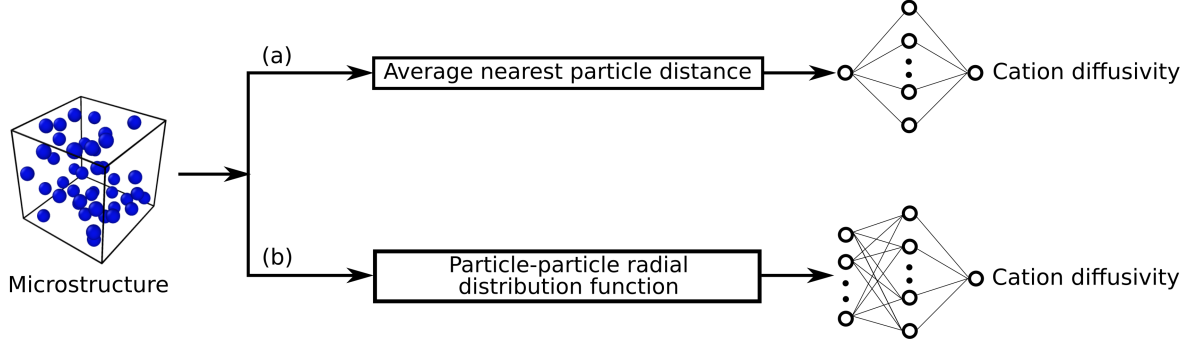
Figure 4: Schematic of the alternative physics-inspired deep-learning models using (a) average nearest particle distance or (b) particle-particle radial distribution function as microstructural inputs to predict cation diffusivity.

scriptors as input features. In one of the methods, we use the average nearest particle distance, reported to be a measure which correlates well with the cation diffusivity for the ion transport model considered in this study.[42] We also explored another surrogate model with nanoparticle-nanoparticle radial distribution function as the input feature to predict cation diffusivity. Although other two-point (particle-particle) correlation functions have been employed as structural descriptors for predicting properties of composites with granular and continuous phases,[24,31,32,53–59] we observe the radial distribution functions to be a more relevant descriptor for the microstructures in our case with uniformly sized nanoparticles (supporting results in SI, Section S6.2). Further details on the architecture of the deep artificial neural networks adopted for the above physics-inspired approaches are provided in SI, Section S6.1. The performance of such models is evaluated on the same training and testing set generated using the methodology discussed in Section 2.1.

From the results displayed in Figure 5, the CNN model is able to furnish more accurate predictions than the physics-inspired models. This suggests that the physics-based descriptors, which do not contain information pertaining to many-body spatial correlations, may be insufficient for identifying the most relevant microstructural features influencing cation diffusivity. For the CNN model, although the convolutional filter size is smaller than the size of a nanoparticle, the spatial correlations between multiple nanoparticles can be captured by the deeper network implemented in this study with four convolutional layers.[60,61] More
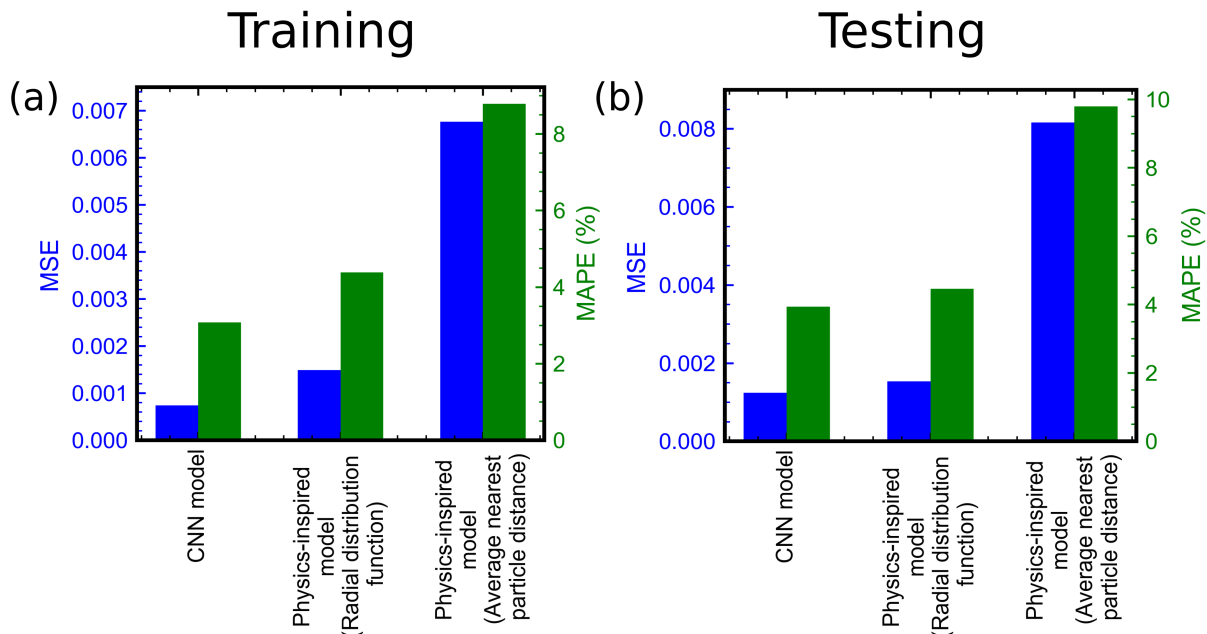
Figure 5: Bar graph for the MSE and MAPE of the predictive models for structures in the originally generated (a) training and (b) testing sets.

specifically, the CNN filters can effectively capture the relevant 3-point and higher-order spatial correlations[40] influencing transport in ways not possible from deep-learning models based on the simpler physics-inspired descriptors.

The quantitative agreement between the CNN predictions and the ground truth diffusivities provides evidence that CNNs are a promising tool for predicting macroscopic properties of two-phase composites comprising spherical nanoparticles. Further, since predicting diffusivity using the CNN model is faster than running brute kMC simulations, it can be an efficient proxy in frameworks that require many evaluations of cation diffusivity. We therefore integrate the CNN models with the topology optimization algorithms which requires calculating cation diffusivity at each step, to help discover new composite materials with desired characteristics and develop even more accurate predictive tools as discussed below.
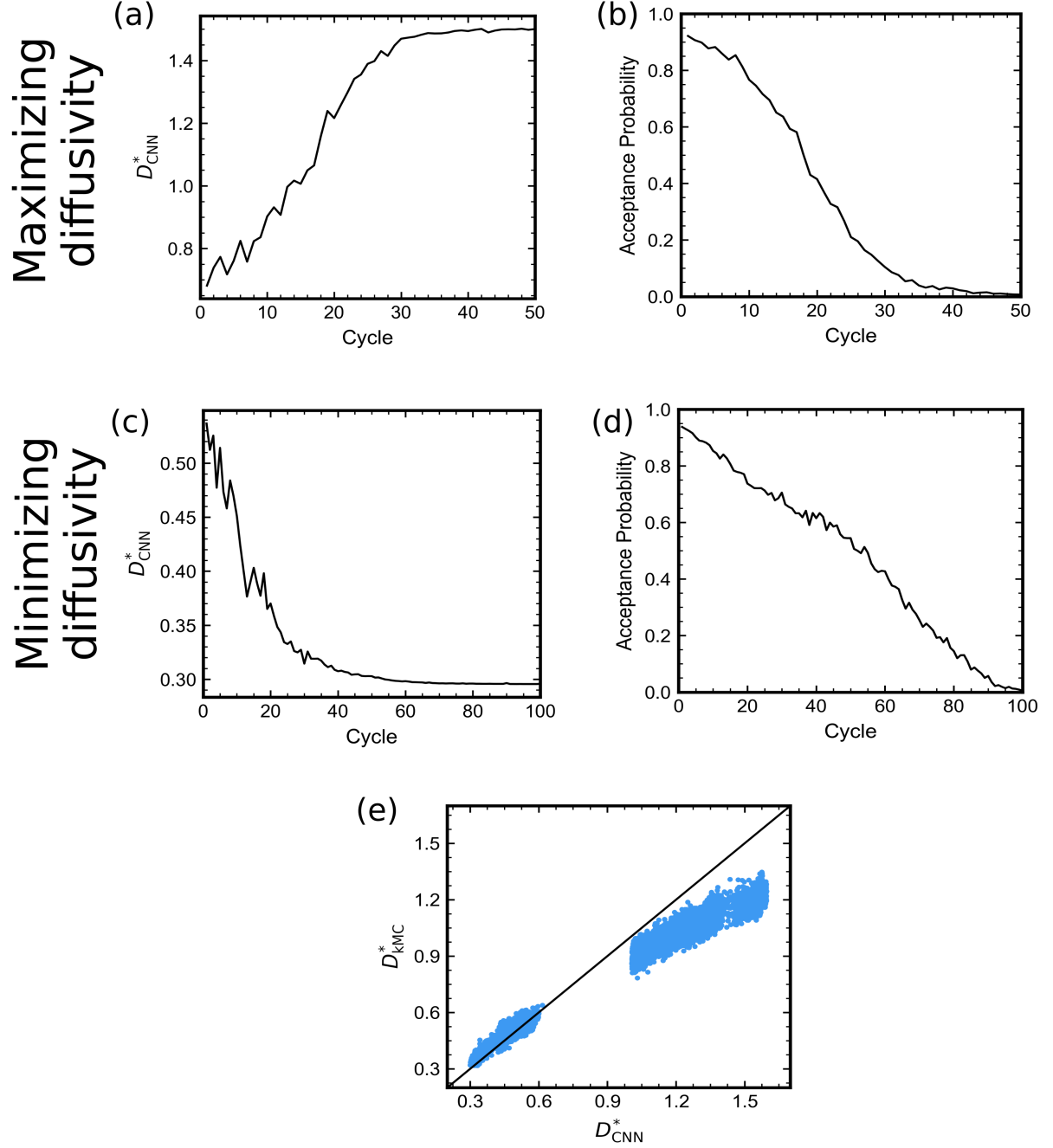
Figure 6: Example of topology optimization using SA. (a) CNN-predicted diffusivity and (b) acceptance probability of a structural change at each SA cycle for diffusivity maximization. (c) CNN-predicted diffusivity and (d) acceptance probability of a structural change at each SA cycle for diffusivity minimization. (e) Parity plot comparing diffusivity obtained via kMC simulation versus the CNN model for randomly chosen structures evaluated during the topology optimizations.

3.2 Topology Optimization for Diffusivity using the CNN Model

Next, we explore the efficacy of using SA optimization with the CNN model to identify a diverse array of microstructures with diffusivities outside the bounds of those observed for structures in the originally generated dataset.

We show results pertaining to two of the 20 independent runs for the SA algorithms used to find microstructures that maximize (or alternatively minimize) cation diffusivity as discussed in Section 2.4. For the SA algorithm to maximize diffusivity, the CNN-predicted diffusivities converge to an optimal value as shown in Figure 6a. From the results displayed in Figure 6b, it is seen that the control parameter D_k^* is changed slowly enough such that the acceptance rate steadily decreases from an initial value of 1 to 0, indicating convergence to the optimal solution. Similarly, the results presented in Figure 6c,d indicate converged solution for the SA algorithm to minimize diffusivity.

Figure 6e shows the comparison between diffusivities predicted by the CNN model and those computed using the kMC simulations for the randomly chosen structures evaluated during the optimization process (as discussed in Section 2.5). It is apparent that, although these diverse microstructures with a wide range of diffusivities were not included in the training dataset, the CNN model estimates the diffusivity for such structures with reasonable accuracy. Furthermore, a Pearson's R (as a measure of linear correlation)[62] of 0.975 between the CNN-predicted and ground truth diffusivities demonstrates the ability of the trained CNN model to identify the relevant spatial features influencing diffusivity, and thereby successfully progress towards optimal microstructures by integrating with SA algorithm.

3.3 Performance of Retrained CNN Model

In this section, we present results for the performance of the CNN model revised using the expanded training dataset comprising the original dataset along with the microstructures identified from the topology optimization runs with CNN-predicted diffusivities outside the bounds of those in the originally generated dataset (as discussed in Section 2.5).
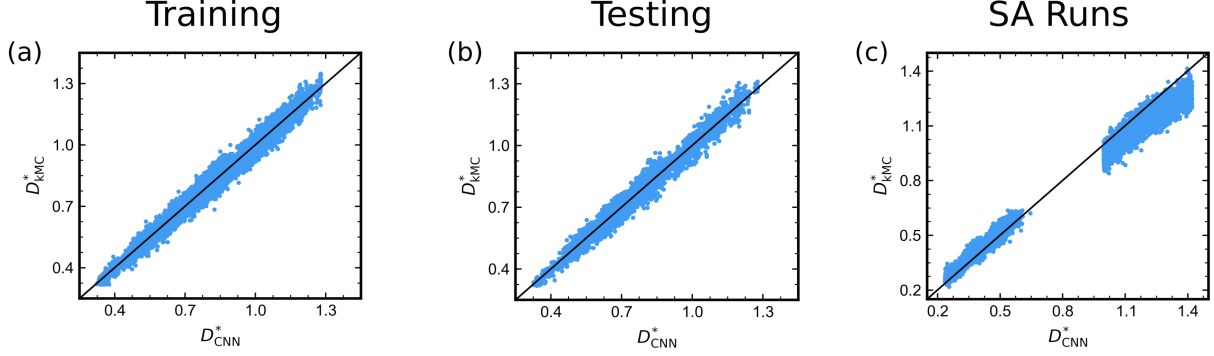
Figure 7: Predictions of retrained CNN model for expanded dataset. Parity plots comparing kMC and CNN-predicted diffusivity for (a) training and (b) testing sets. (c) Parity plots comparing kMC and CNN-predicted diffusivity for randomly chosen structures evaluated during the topology optimization SA runs with the retrained CNN model.

Figure 7 shows parity plots comparing diffusivity computed from kMC simulations to that predicted from the retrained CNN model. We observe excellent agreement with an MSE/MAPE of 8.978×10^{-4} / 3.147% and 1.164×10^{-3} / 3.632% for structures in the modified training and testing sets, respectively. We further report the model predictions for the structures discovered on repeating the topology optimization runs using SA (as described in Section 2.4) with the revised CNN model to estimate diffusivities. From the results shown in Table 1, we observe improved accuracy with the revised CNN model for the structures screened during the SA runs for topology optimization. Further, a Pearson's R close to one (R = 0.985) is observed between the predicted and ground truth values.

In the next section, we present results which explore the extent to which the CNN model encodes information about the presence of nanoparticles by testing its ability to predict cation diffusivities for microstructures with nanoparticle volume fractions lower and higher than those in the training dataset.

Table 1: Comparison of prediction accuracy for structures evaluated during the SA algorithm runs

Model	MSE/MAPE
CNN model trained with original dataset	3.611×10^{-2} / 15.634%
CNN model retrained with expanded dataset	5.739×10^{-3} / 7.133%

4 CNN Predictions for different Nanoparticle Loadings

The success of the CNN model studied here for predicting cation diffusivity in nanocomposites with spherical nanoparticles clearly hinges on its ability to detect how nanoparticle positions and the related positional interparticle correlations influence diffusivity. Here, by modifying the types of microstructures we input into the revised CNN model, we aim to examine whether the CNN filters can adequately recognize and account for the impact of added or deleted nanoparticles, and accordingly predict the corresponding cation diffusivity.

Based on the ion transport model considered in this study, the cation diffusivity is expected to be significantly influenced by the nanoparticle volume fraction.[42] Since the effect of nanoparticle volume fraction on the cation diffusivity was not explicitly introduced to the CNN model during the training process, we interpret what the model learns by studying the accuracy of the CNN model predictions for microstructures of different volume fractions. To that end, nanoparticles were randomly added to (removed from) each structure in the
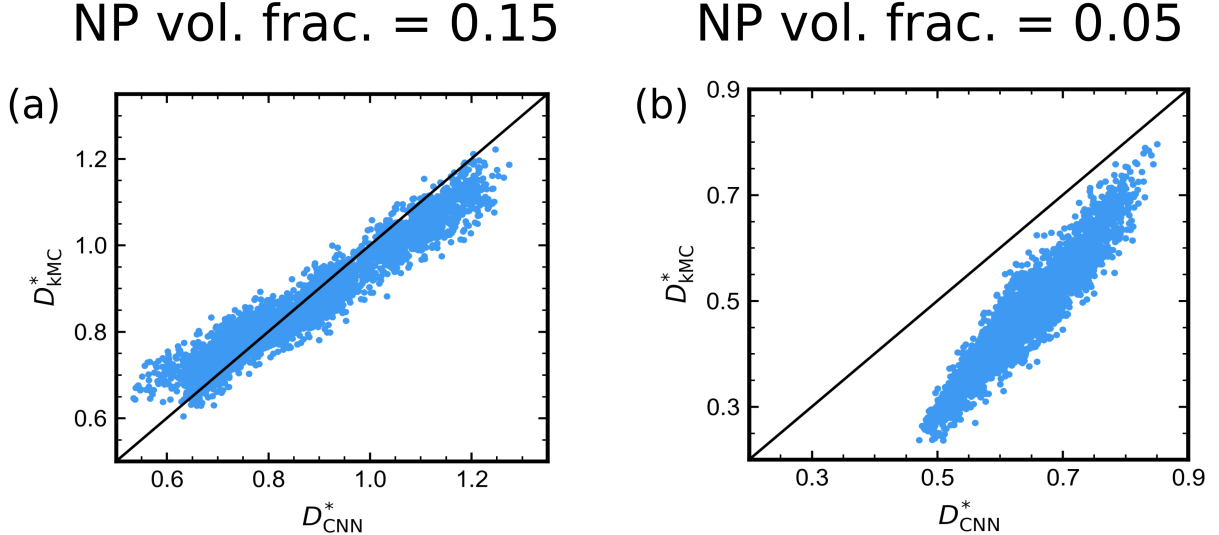

Figure 8: Predictions of retrained CNN model for different nanoparticle (NP) loadings. Parity plots comparing kMC and CNN-predicted diffusivity for microstructures with (a) 15% NP loading and (b) 5% NP loading, by volume.

Table 2: Prediction accuracy for structures at different nanoparticle loadings

Nanoparticle volume fraction	MSE/MAPE	Pearson's R
0.15	2.95×10^{-3} / 5.008%	0.967
0.05	2.863×10^{-2} / 37.069%	0.928

testing set to generate microstructures with a nanoparticle volume fraction of 0.15 (0.05) while ensuring nonoverlap between nanoparticles. Figure 8 shows parity plots comparing the CNN-predicted and kMC-calculated diffusivities for the modified input structures. For the microstructures with 15% nanoparticle volume fraction, although the volume occupied by the nanoparticles is higher than that for the structures in the training dataset (leading to increase in the activation of the model due to the increase in the number of voxels representated as 1s in the image), excellent agreement is observed (Table 2). This suggests that the convolutional filters in the multiple layers of the deep network are able to accurately identify the location of nanoparticles in the microstructues, and characterize the relevant spatial correlations between multiple nanoparticle influencing cation diffusivity. We hypothesize the overpredicted diffusivity values for structures with 5% nanoparticle volume fraction to be a result of the inability of the learned CNN filters to quantify the effect of large voids in the microstructure due to particle deletions, which are not prevalent in the training structures with 10% nanoparticle volume fraction.

Nonetheless, the Pearson's R values for the modified structures, combined with the reasonable prediction accuracy (Table 2), demonstrates the potential for integrating the CNN model with topology optimization algorithms to accurately identify optimal microstructures at different nanoparticle loadings. However, we do acknowledge that the prediction accuracy at different nanoparticle volume fractions is expected to be better if the CNN model is explicitly trained using microstructures with those corresponding nanoparticle loadings.
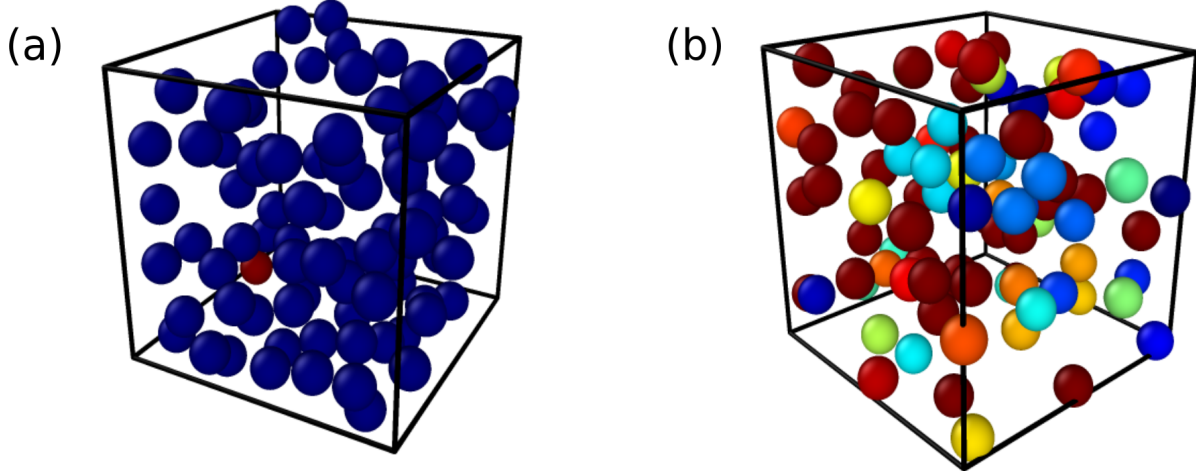
Figure 9: Snapshots of nanoparticle configurations with (a) maximum, and (b) minimum ground truth diffusivity. The nanoparticle volume fraction is 0.1. For visual clarity, nanoparticles within the same cluster (identified by optimal separation distance of approximately 14 voxels between neighboring particles) are shown by the same color to highlight the resulting percolating network of nanoparticles in (a), and the isolated clusters of relatively closely spaced nanoparticles in (b).

5 Effect of Structural Features on Cation Diffusivity

Although the CNN and other deep learning models based on physics-inspired approaches present an avenue for quantitative structure–property linkage, understanding the relationship between the structural descriptors and the property of interest is difficult due to the "black box" nature of the deep learning models. In this section, we probe the influence of the structural descriptors on cation diffusivity using data-driven approaches, and we examine whether there are physical mechanisms underlying the optimal microstructures obtained using the combination of the CNN model and the topology optimization algorithm.

We first qualitatively comment on the structural characteristics of the optimal morphologies from a visual perspective. Figure 9 depicts snapshots of nanoparticle configurations exhibiting maximum and minimum diffusivity. Explicitly, we observe the structure with maximum cation diffusivity to possess a stringlike network of nanoparticles, percolated in all three directions. The individual particles in the network are separated from their nearest neighbors by spacings favorable for interparticle transport (at approximately 14 voxels)
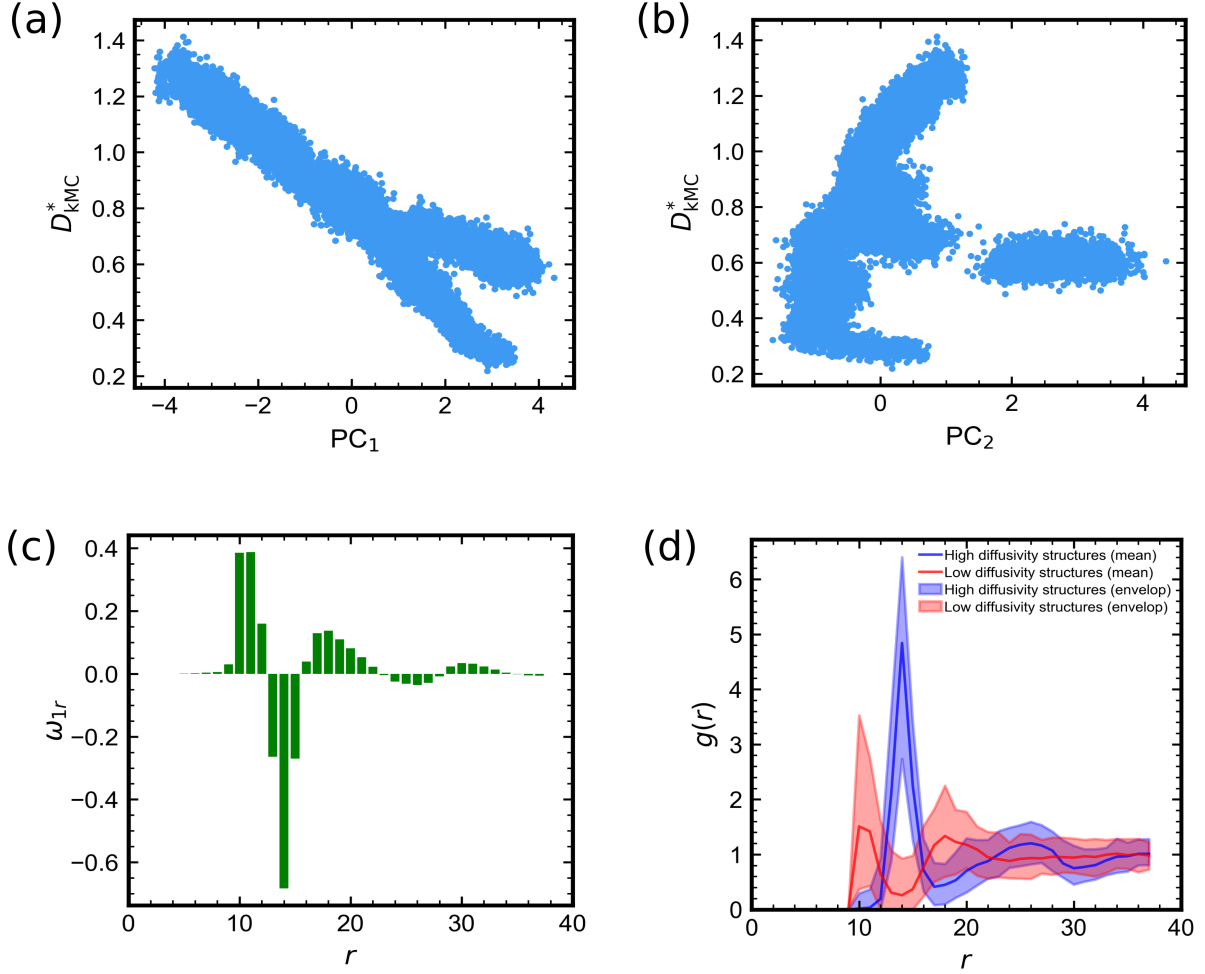
22

Figure 10: Correlation between the ground truth (i.e., kMC simulation) diffusivities and (a) PC_1, (b) PC_2 for all the structures probed in this study. (c) Feature weights for PC_1, and (d) $g(r)$ values for the high and low diffusivity structures.

according to the underlying cation transport model. In contrast, the configuration with minimum cation diffusivity displays an unpercolated microstructure with isolated clusters of nanoparticles where the adjacent particles are separated by a distance smaller than 14 voxels, configurations previously shown in the cation transport model to exhibit significant interdigitation of the surface-functionalizing ligands.[42]

To provide a more quantitative dependence of cation diffusivity on structural features, we perform principal component analysis (PCA) on a dataset consisting of nanoparticle-nanoparticle radial distribution function $g(r)$ (considering the central voxel of each nanoparticle) of the microstructures probed in this study. The radial distribution functions are

evaluated for integer r values from 0 to 38 voxels. The maximum value of r corresponds to half the length of the cubic box (L) comprising the microstructure. The ith principal component (PC_i) is given by a linear combination of the original features $g(r), r = 0, 1, ..., 38$

$$PC_i = \sum_{r=0}^{38} \omega_{ir} g(r) \tag{6}$$

where w_{ir} denotes the weight of the feature $g(r)$ for PC_i. Based on PCA, the first and second principal components (PC_1 and PC_2) capture approximately 67% and 13% of the total variance, respectively. Figure 10a clearly displays a negative correlation between the PC_1 value of a structure and its corresponding cation diffusivity with a Pearson's R of 0.93. However, no significant correlation is observed between the cation diffusivity and any of the other principal components, with a maximum absolute Pearson's R of 0.57 for PC_2 (Figure 10b). We observe both positive and negative feature weights for PC_1 as shown in Figure 10c depending on the nanoparticle separation. Since there exists a strong negative correlation between the PC_1 value and the cation diffusivity, and $g(r) \geq 0$, the features with negative (positive) weight can be interpreted as important structural characteristics that correspond to high (low) cation diffusivity.

Figure 10d shows the comparison of $g(r)$ values for structures corresponding to both the highest 10% and the lowest 10% of diffusivities. Accordingly, for the high and low diffusivity structures, significant peaks are observed for the structural features with negative and positive weights, respectively. From a physical perspective, such trends can be understood based on the cation transport model considered in this study.[42] Specifically, the initial features with negative weights for PC_1 correspond to the narrow range of nanoparticle separations where cations at the surface of one particle can readily transport to the surface of a neighboring particle via diffusion. The initial features with positive weights for PC_1 reflect the relatively slower cation transport from one particle to another that occurs when adjacent particles are separated by a distance smaller than the optimal interparticle spacings.

To summarize, application of PCA to the dataset of microstructure radial distribution functions from this topology optimization study, together with direct visualization of optimal microstructures, allows us to identify that for the cation transport model considered in this study, *nearest neighbor spacing* and *percolation* of nanoparticles are the main structural characteristics significantly influencing the cation diffusivity. However, we recall the results of Section 3.1 which established that 3- and higher-particle correlations have significant consequences for cation transport. Hence, our results in this study point to the observation that while physics-based models can be useful in understanding and predicting the morphology dependencies of different properties, CNN-based deep learning models can potentially expand such capablties and allow us to probe configurations which may not be subsumed within a purely physics-based approach.

6   Conclusions

We have developed a CNN-based deep learning model for predicting the cation diffusivity through a 3D microstructure consisting of monodisperse spherical nanoparticles. The CNN approach not only achieves a high prediction accuracy, but also outperforms other physics-inspired deep learning models. We surmise that the latter is due to the ability of CNN filters to capture the relevant many-body spatial correlations not accounted for in the simple physics-based descriptors. On combining the trained CNN model with a simulated annealing algorithm for topology optimization, we achieve accelerated discovery of microstructures exhibiting ground truth diffusivities outside the domain of those observed for structures in the generated training dataset. Incorporating these additional observations to retrain the CNN model leads to further improvement in the prediction accuracy for a wide range of nanoparticle microstructures screened during the topology optimization runs. We observe a 41.3% increase in the maximum diffusivity compared to that in the initial training dataset generated using a combination of stochastic algorithm with physically intuited biasing. Ap-

plying PCA to the dataset of structures revealed important physical features influencing cation diffusivity, thus providing a physical rationale for the performance of optimal morphologies. Such a data-driven analysis allows for a better interpretation of the quantitative effect of the cation transport model on the property of interest, i.e. cation diffusivity.

Overall, this work demonstrates the potential of CNN as a feature-engineering-free, high accuracy deep learning model to quantitatively link the complex structure–property relationships in composites with uniformly sized spherical particles. The strategy adopted in this study of combining the CNN-based deep learning model with a topology optimization algorithm can be generalized for accelerated prediction and optimization of nanocomposite properties, if sufficient computational or experimental material data are available to train the model. Further, such an approach to identify the optimal structures can be subsequently combined with inverse methods to determine the nanoparticle interactions or building blocks that promote self-assembly of the corresponding target structures. Broadly, our work demonstrates the potential of deep learning-based strategies to efficiently navigate the high-dimensional design space to discover/design materials with target properties.

Supporting Information Available

Multiscale simulations to model cation transport (S1) with MD simulation details (S1.1), force field details for MD simulations (S1.2) and on-lattice kMC simulation details (S1.3); Constraints applied to generate dataset with diverse nanoparticle microstructures (S2); Methodology for mapping nanoparticle microstructure to 3D binary image (S3); Hyperparameters for training deep neural network models (S4); Supporting results on the predictive performance of CNN model with $75 \times 75 \times 75$ binary image input (S5.1), predictive accuracy for different CNN architectures (S5.2), loss curves for training CNN model (S5.3); Supporting results on the artificial neural network architectures (S6.1) and predictive performance (S6.2) for different physics-inspired models.

Acknowledgement

References

(1) Austin Suthanthiraraj, S.; Johnsi, M. Nanocomposite polymer electrolytes. *Ionics* **2017**, *23*, 2531–2542.

(2) Yao, P.; Yu, H.; Ding, Z.; Liu, Y.; Lu, J.; Lavorgna, M.; Wu, J.; Liu, X. Review on Polymer-Based Composite Electrolytes for Lithium Batteries. *Front. Chem.* **2019**, *7*, 522.

(3) Pinto, D.; Bernardo, L.; Amaro, A.; Lopes, S. Mechanical properties of epoxy nanocomposites using titanium dioxide as reinforcement – A review. *Constr. Build. Mater.* **2015**, *95*, 506 – 524.

(4) Tjong, S. Structural and mechanical properties of polymer nanocomposites. *Mater. Sci. Eng. R Rep.* **2006**, *53*, 73 – 197.

(5) Silvestre, J.; Silvestre, N.; de Brito, J. An Overview on the Improvement of Mechanical Properties of Ceramics Nanocomposites. *J. Nanomater.* **2015**, *2015*, 106494.

(6) Nguyen, T.-P. Polymer-based nanocomposites for organic optoelectronic devices. A review. *Surf. Coat. Technol.* **2011**, *206*, 742 – 752.

(7) Zhan, C.; Yu, G.; Lu, Y.; Wang, L.; Wujcik, E.; Wei, S. Conductive polymer nanocomposites: a critical review of modern advanced devices. *J. Mater. Chem. C* **2017**, *5*, 1569–1585.

(8) Peng, F.; Lu, L.; Sun, H.; Wang, Y.; Liu, J.; Jiang, Z. Hybrid Organic–Inorganic Membrane: Solving the Tradeoff between Permeability and Selectivity. *Chem. Mater.* **2005**, *17*, 6790–6796.

(9) Merkel, T. C.; Freeman, B. D.; Spontak, R. J.; He, Z.; Pinnau, I.; Meakin, P.; Hill, A. J. Ultrapermeable, Reverse-Selective Nanocomposite Membranes. *Science* **2002**, *296*, 519–522.

(10) Cong, H.; Radosz, M.; Towler, B. F.; Shen, Y. Polymer–inorganic nanocomposite membranes for gas separation. *Sep. Purif. Technol.* **2007**, *55*, 281 – 291.

(11) Mogurampelly, S.; Sethuraman, V.; Pryamitsyn, V.; Ganesan, V. Influence of nanoparticle-ion and nanoparticle-polymer interactions on ion transport and viscoelastic properties of polymer electrolytes. *J. Chem. Phys.* **2016**, *144*, 154905.

(12) Mogurampelly, S.; Ganesan, V. Effect of Nanoparticles on Ion Transport in Polymer Electrolytes. *Macromolecules* **2015**, *48*, 2773–2786.

(13) Singha, S.; Jana, T. Proton-Conducting Channels in Polybenzimidazole Nanocomposites. *J. Indian Inst. Sci.* **2016**, *96*, 351–364.

(14) Singha, S.; Jana, T. Self-Assembly of Nanofillers in Improving the Performance of Polymer Electrolyte Membrane. *Macromol. Symp.* **2016**, *369*, 49–55.

(15) Singha, S.; Jana, T. Structure and Properties of Polybenzimidazole/Silica Nanocomposite Electrolyte Membrane: Influence of Organic/Inorganic Interface. *ACS Appl. Mater. Interfaces* **2014**, *6*, 21286–21296.

(16) Akcora, P.; Liu, H.; Kumar, S. K.; Moll, J.; Li, Y.; Benicewicz, B. C.; Schadler, L. S.; Acehan, D.; Panagiotopoulos, A. Z.; Pryamitsyn, V. et al. Anisotropic self-assembly of spherical polymer-grafted nanoparticles. *Nat. Mater.* **2009**, *8*, 354–359.

(17) Kadulkar, S.; Banerjee, D.; Khabaz, F.; Bonnecaze, R. T.; Truskett, T. M.; Ganesan, V. Influence of morphology of colloidal nanoparticle gels on ion transport and rheology. *J. Chem. Phys.* **2019**, *150*, 214903.

(18) Sherman, Z. M.; Howard, M. P.; Lindquist, B. A.; Jadrich, R. B.; Truskett, T. M. Inverse methods for design of soft materials. *J. Chem. Phys.* **2020**, *152*, 140902.

(19) Ferguson, A. L. Machine learning and data science in soft materials engineering. *J. Phys.: Condens. Matter* **2017**, *30*, 043002.

(20) Bai, C.; Zhang, G.; Qiu, Y.; Leng, X.; Tian, M. Direct nanofluids configuration optimization based on the evolutionary topology optimization method. *Int. J. Heat Mass Transf.* **2018**, *117*, 201 – 210.

(21) Dugan, N.; Erkoç, Ş. Genetic Algorithms in Application to the Geometry Optimization of Nanoparticles. *Algorithms* **2009**, *2*, 410–428.

(22) Ferrando, R.; Fortunelli, A.; Johnston, R. L. Searching for the optimum structures of alloy nanoclusters. *Phys. Chem. Chem. Phys.* **2008**, *10*, 640–649.

(23) Johnston, R. L. Evolving better nanoparticles: Genetic algorithms for optimising cluster geometries. *Dalton Trans.* **2003**, 4193–4207.

(24) Gupta, A.; Cecen, A.; Goyal, S.; Singh, A. K.; Kalidindi, S. R. Structure–property linkages using a data science approach: Application to a non-metallic inclusion/steel composite system. *Acta Mater.* **2015**, *91*, 239 – 254.

(25) Ebikade, E. O.; Wang, Y.; Samulewicz, N.; Hasa, B.; Vlachos, D. Active learning-driven quantitative synthesis–structure–property relations for improving performance

and revealing active sites of nitrogen-doped carbon for the hydrogen evolution reaction. *React. Chem. Eng.* **2020**, *5*, 2134 – 2147.

(26) Ganapathysubramanian, B.; Zabaras, N. Modeling diffusion in random heterogeneous media: Data-driven models, stochastic collocation and the variational multiscale method. *J. Comput. Phys.* **2007**, *226*, 326 – 353.

(27) Barman, S.; Rootzén, H.; Bolin, D. Prediction of diffusive transport through polymer films from characteristics of the pore geometry. *AIChE J.* **2019**, *65*, 446–457.

(28) Neumann, M.; Stenzel, O.; Willot, F.; Holzer, L.; Schmidt, V. Quantifying the influence of microstructure on effective conductivity and permeability: Virtual materials testing. *Int. J. Solids Struct.* **2020**, *184*, 211 – 220.

(29) Stenzel, O.; Pecho, O.; Holzer, L.; Neumann, M.; Schmidt, V. Predicting effective conductivities based on geometric microstructure characteristics. *AIChE J.* **2016**, *62*, 1834–1843.

(30) J.H. van der Linden, J. H.; Narsilio, G. A.; Tordesillas, A. Machine learning framework for analysis of transport through complex networks in porous, granular media: A focus on permeability. *Phys. Rev. E* **2016**, *94*, 022904.

(31) Röding, M.; Ma, Z.; Torquato, S. Predicting permeability via statistical learning on higher-order microstructural information. *Sci. Rep.* **2020**, *10*, 15239.

(32) Patel, D. K.; Parthasarathy, T.; Przybyla, C. Predicting the effects of microstructure on matrix crack initiation in fiber reinforced ceramic matrix composites via machine learning. *Compos. Struct.* **2020**, *236*, 111702.

(33) Lecun, Y.; Bottou, L.; Bengio, Y.; Haffner, P. Gradient-based learning applied to document recognition. *Proc. IEEE* **1998**, *86*, 2278–2324.

(34) Wu, H.; Fang, W.-Z.; Kang, Q.; Tao, W.-Q.; Qiao, R. Predicting Effective Diffusivity of Porous Media from Images by Deep Learning. *Sci. Rep.* **2019**, *9*, 20387.

(35) Pokuri, B. S. S.; Ghosal, S.; Kokate, A.; Sarkar, S.; Ganapathysubramanian, B. Interpretable deep learning for guided microstructure-property explorations in photovoltaics. *NPJ Comput. Mater.* **2019**, *5*, 95.

(36) Wu, J.; Yin, X.; Xiao, H. Seeing permeability from images: fast prediction with convolutional neural networks. *Sci. Bull.* **2018**, *63*, 1215 – 1222.

(37) Karimpouli, S.; Tahmasebi, P. Image-based velocity estimation of rock using Convolutional Neural Networks. *Neural Netw.* **2019**, *111*, 89 – 97.

(38) Wang, Y.; Zhang, M.; Lin, A.; Iyer, A.; Prasad, A. S.; Li, X.; Zhang, Y.; Schadler, L. S.; Chen, W.; Brinson, L. C. Mining structure–property relationships in polymer nanocomposites using data driven finite element analysis and multi-task convolutional neural networks. *Mol. Syst. Des. Eng.* **2020**, *5*, 962–975.

(39) Yang, Z.; Yabansu, Y. C.; Al-Bahrani, R.; keng Liao, W.; Choudhary, A. N.; Kalidindi, S. R.; Agrawal, A. Deep learning approaches for mining structure-property linkages in high contrast composites from simulation datasets. *Comput. Mater. Sci.* **2018**, *151*, 278 – 287.

(40) Cecen, A.; Dai, H.; Yabansu, Y. C.; Kalidindi, S. R.; Song, L. Material structure-property linkages using three-dimensional convolutional neural networks. *Acta Mater.* **2018**, *146*, 76 – 84.

(41) Yang, Z.; Yabansu, Y. C.; Jha, D.; keng Liao, W.; Choudhary, A. N.; Kalidindi, S. R.; Agrawal, A. Establishing structure-property localization linkages for elastic deformation of three-dimensional high contrast composites using deep learning approaches. *Acta Mater.* **2019**, *166*, 335 – 345.

(42) Kadulkar, S.; Milliron, D. J.; Truskett, T. M.; Ganesan, V. Transport Mechanisms Underlying Ionic Conductivity in Nanoparticle-Based Single-Ion Electrolytes. *J. Phys. Chem. Lett.* **2020**, *11*, 6970–6975.

(43) Schaefer, J. L.; Yanga, D. A.; Archer, L. A. High Lithium Transference Number Electrolytes via Creation of 3-Dimensional, Charged, Nanoporous Networks from Dense Functionalized Nanoparticle Composites. *Chem. Mater.* **2013**, *25*, 834–839.

(44) Zhao, H.; Jia, Z.; Yuan, W.; Hu, H.; Fu, Y.; Baker, G. L.; Liu, G. Fumed Silica-Based Single-Ion Nanocomposite Electrolyte for Lithium Batteries. *ACS Appl. Mater. Interfaces* **2015**, *7*, 19335–19341.

(45) Widom, B. Random Sequential Addition of Hard Spheres to a Volume. *J. Chem. Phys.* **1966**, *44*, 3888–3894.

(46) Voulodimos, A.; Doulamis, N.; Doulamis, A.; Protopapadakis, E. Deep Learning for Computer Vision: A Brief Review. *Comput. Intell. Neurosci.* **2018**, *2018*, 7068349.

(47) Chollet, F., et al. Keras. `https://github.com/fchollet/keras/` (accessed August 22, 2020).

(48) Balling, R. J. Optimal Steel Frame Design by Simulated Annealing. *J. Struct. Eng.* **1991**, *117*, 1780–1795.

(49) Bennage, W. A.; Dhingra, A. K. Single and multiobjective structural optimization in discrete-continuous variables using simulated annealing. *Int. J. Numer. Meth. Eng.* **1995**, *38*, 2753–2773.

(50) Elperin, T. Monte Carlo structural optimization in discrete variables with annealing algorithm. *Int. J. Numer. Meth. Eng.* **1988**, *26*, 815–821.

(51) Botu, V.; Ramprasad, R. Adaptive machine learning framework to accelerate ab initio molecular dynamics. *Int. J. Quantum Chem.* **2015**, *115*, 1074–1083.

(52) Ren, F.; Ward, L.; Williams, T.; Laws, K. J.; Wolverton, C.; Hattrick-Simpers, J.; Mehta, A. Accelerated discovery of metallic glasses through iteration of machine learning and high-throughput experiments. *Sci. Adv.* **2018**, *4*, eaaq1566.

(53) Altschuh, P.; Yabansu, Y. C.; Hötzer, J.; Selzer, M.; Nestler, B.; Kalidindi, S. R. Data science approaches for microstructure quantification and feature identification in porous membranes. *J. Membr. Sci.* **2017**, *540*, 88 – 97.

(54) Choudhury, A.; Yabansu, Y. C.; Kalidindi, S. R.; Dennstedt, A. Quantification and classification of microstructures in ternary eutectic alloys using 2-point spatial correlations and principal component analyses. *Acta Mater.* **2016**, *110*, 131 – 141.

(55) Khosravani, A.; Cecen, A.; Kalidindi, S. R. Development of high throughput assays for establishing process-structure-property linkages in multiphase polycrystalline metals: Application to dual-phase steels. *Acta Mater.* **2017**, *123*, 55 – 69.

(56) Yabansu, Y. C.; Steinmetz, P.; Hötzer, J.; Kalidindi, S. R.; Nestler, B. Extraction of reduced-order process-structure linkages from phase-field simulations. *Acta Mater.* **2017**, *124*, 182 – 194.

(57) Jung, J.; Yoon, J. I.; Park, H. K.; Kim, J. Y.; Kim, H. S. An efficient machine learning approach to establish structure-property linkages. *Comput. Mater. Sci.* **2019**, *156*, 17 – 25.

(58) Latypov, M. I.; Kalidindi, S. R. Data-driven reduced order models for effective yield strength and partitioning of strain in multiphase materials. *J. Comput. Phys.* **2017**, *346*, 242 – 261.

(59) Paulson, N. H.; Priddy, M. W.; McDowell, D. L.; Kalidindi, S. R. Reduced-order structure-property linkages for polycrystalline microstructures based on 2-point statistics. *Acta Mater.* **2017**, *129*, 428 – 438.

(60) He, K.; Sun, J. Convolutional neural networks at constrained time cost. *2015 IEEE Conference on Computer Vision and Pattern Recognition (CVPR)* **2015**, 5353–5360.

(61) Szegedy, C.; Wei Liu,; Yangqing Jia,; Sermanet, P.; Reed, S.; Anguelov, D.; Erhan, D.; Vanhoucke, V.; Rabinovich, A. Going deeper with convolutions. *2015 IEEE Conference on Computer Vision and Pattern Recognition (CVPR)* **2015**, 1–9.

(62) Pearson, K. Notes on regression and inheritance in the case of two parents. *Proc. R. Soc. Lond.* **1895**, *58*, 240–242.

Graphical TOC Entry